Available online at www.sciencedirect.com
ScienceDirect
International Journal of Heat and Mass Transfer 50 (2007) 4975–4985
International Journal of HEAT and MASS TRANSFER
www.elsevier.com/locate/ijhmt

The impact of air saturation on the flow structure beneath air–water interface during natural convection

Syed J.K. Bukhari, M.H. Kamran Siddiqui *

Department of Mechanical and Industrial Engineering, Concordia University, Montreal, QC, Canada H3G 1M8

Received 27 January 2007; received in revised form 29 June 2007
Available online 22 October 2007

Abstract

We report on results from an experimental study conducted to investigate the impact of air saturation on the turbulent structure beneath air–water interface. Particle image velocimetry (PIV) was used to measure the two dimensional velocity fields beneath the water surface. The results show that air saturation has a significant impact on the waterside turbulent structure. As the air becomes saturated, the magnitudes of the horizontal and vertical turbulent velocities are decreased by factors of 5 and 2.5, respectively. It was argued that in addition to the surface heat flux, the waterside flow field is also influenced by the airside velocity via the air–water interface. The latent heat flux at the saturation state is not equal to zero. The film condensation on the tank walls at the saturation state is found to be responsible for the latent heat flux. The spectral analysis shows that both the horizontal and vertical turbulent motions are much weaker than that for the unsaturated case. For the saturated case, the range of the turbulent motions responsible for working against buoyancy forces is smaller than that for the unsaturated case. It was concluded that during natural convection, when the turbulence is relatively weak, in addition to the buoyancy subrange, another subrange exists within the inertial subrange, where the turbulent motions are simply convected by the buoyancy forces and that the energy interaction is highly dependent on the energy of the turbulent motions and the magnitude of the buoyancy forces.

1. Introduction

Natural convection plays an important role in many engineering and environmental applications. It is a process during which the mass and heat exchange between air and water takes place without any external influence. The natural convection process in an air–water system is significantly influenced by the evaporation at the interface. The evaporation causes the latent heat transfer from the water surface which results in the formation of a cool water layer at the interface. This cool and dense water layer becomes unstable and falls through the warm less dense water underneath. The warmer water rises to replace the falling cold water to satisfy the mass conservation. When the bulk water is warmer than the bulk air, heat also transfers across the interface in the form of sensible heat. The natural convection process beneath the air–water interface is turbulent and the resulting velocity fields are complex [1]. Under normal conditions during natural convection when the air is not saturated, the latent heat transfer constitutes up to 90% of the heat transfer across the air–water interface [2,3]. Thus, the relative humidity on the airside plays a crucial role in controlling the bulk of the heat transfer across the air–water interface.

There are only few studies reported in the literature which investigated the flow behavior beneath the air–water interface during natural convection. Bukhari and Siddiqui [4] numerically investigated the airside and waterside flow behavior in a coupled air–water system undergoing natural convection. They simulated the flow fields for unstable and stable thermal stratifications, and neutral condition. They found that during unstable thermal stratification, the magnitude of the root-mean-square (RMS) airside velocity is an order of magnitude higher than the RMS waterside

* Corresponding author. Tel.: +1 514 848 2424x7940; fax: +1 514 848 3175.
E-mail address: siddiqui@encs.concordia.ca (M.H. Kamran Siddiqui).

0017-9310/$ - see front matter © 2007 Elsevier Ltd. All rights reserved.
doi:10.1016/j.ijheatmasstransfer.2007.09.003

velocity. However, for neutral and stable cases, the velocity magnitudes are comparable for air and water. They concluded that the bulk air and water temperature difference play an important role in controlling the flow fields.

Volino and Smith [2] used infrared imagery and digital particle image velocimetry (DPIV) to measure surface temperature and subsurface velocity field during natural convection for neutral and unstable cases. Their flux estimates showed that approximately 15% of the heat flux across the air–water interface was driven by the temperature gradient from water to air while 85% was due to evaporation from the water surface. They found that the cool water surface layer plunges into the warm bulk water in sheet like plumes. They also found that the magnitude of RMS horizontal and vertical velocities increased with the heat flux. Flack et al. [5] measured surface temperature and subsurface turbulence during evaporative convection using infrared imagery and two component laser Doppler velocimetry, respectively. They conducted experiments with water temperature 14-16 °C above the bulk air temperature for two different surface conditions; one with a clean surface (shear free condition) and the other in the presence of a surfactant monolayer. They observed that the near-surface turbulent intensities were higher beneath the clean surface as compared to the contaminated surface and that this difference decreased with the distance from the free surface.

Bukhari and Siddiqui [1] experimentally investigated the turbulent structure beneath the air–water interface during natural convection using DPIV. The experiments were conducted for three cases. Two cases correspond to the unstable thermal stratification with bulk water temperature 13 °C and 7 °C warmer than the bulk air and the third case correspond to the neutral case. Based on the analysis of the two-dimensional turbulent velocity fields they argued that during natural convection, the waterside flow field is three-dimensional that undergoes different flow interactions locally, which result in the formation of complex flow patterns. They also observed self similar behavior in the turbulent velocities for different cases and showed that the scaling parameters used for the flow above a heated solid wall are also suitable for the flow field beneath the evaporative interface. From the spectral analysis they showed that the buoyancy subrange exists within the inertial subrange when the turbulent motions are strong enough to work against the buoyancy forces. They also observed that the range of the length scales of the turbulent motions involved in the interactions with the buoyancy forces does not vary with the heat flux. However, the range of timescales of the turbulent motion reduces with a decrease in the heat flux.

All these studies were focused on the investigation of the flow characteristics when the air above the water surface is unsaturated. The typical relative humidity range in these studies was 30–45%. Thus, the latent heat transfer was the dominant heat transfer mode in these studies. In some engineering and environmental applications, the air above the water surface is saturated or could reach saturation state under certain circumstances. For example, in natural-draft cooling towers used in process, HVAC or other related industries, the air above the water pool is saturated. Similarly, in nuclear power plants, any interruption in the water cooling system of the spent fuel storage bays would result in the rise of the water temperature due to decay heat of the fuel, creating saturation condition in the air above the water pool. From environmental aspect, mixing of warmer air from the land with the relatively cool air above the water bodies such as oceans and lakes, results in an increased relative humidity which could create foggy conditions above the water surface.

In applications where the air above the water is saturated or in cases where temporary air saturation occurs, it is important to understand the impact of air-saturation on the waterside flow behavior, as the waterside turbulent velocity field has a significant impact on the flow structure and the air–water heat and mass exchange. For example, the upper ocean circulation has a significant impact on the air–sea heat exchange and the uptake of environmental gases such as CO_2 and oxygen. However, as far as the authors know, no study has reported the impact of air saturation on the flow behavior underneath the air–water interface. The present study is directed towards understanding the behavior of the waterside velocity fields when the air becomes saturated. The data for the saturated air case were acquired during the same set of experiments reported in Bukhari and Siddiqui [1]. However, Bukhari and Siddiqui [1] reported the results for the unsaturated case only.

2. Experimental setup

The experiments were conducted in a glass tank, 60 cm long, 30 cm wide and 50 cm deep. The tank was filled with clean tap water. For all experimental runs the water depth was maintained at 26 cm and the bulk air temperature was 23 °C. During the experimental runs for unsaturated air cases, the tank top was left open to allow evaporation into the room air [1]. For the measurements under saturated conditions, the tank top was covered with a lid to reach 100% saturation inside the tank. The present study is focused on investigating the impact of air saturation when air and water fields are unstably stratified. Therefore, for saturation study two experimental cases are considered that corresponds to the bulk water temperatures of 36 °C and 30 °C. For each case, water was heated to a temperature 3–4 °C above the set bulk water temperature, the tracer particles were added, the water was stirred thoroughly, and then it allowed to settle down to a quasi-steady state. The data acquisition for the unsaturated case was started as soon as the bulk water temperature reached the set temperature. Immediately after the completion of the data acquisition for the unsaturated case, the top of the tank was covered with a lid to reach the saturation state. The saturation condition inside the tank reached within 1 min

for the bulk water temperature of 36 °C, while it took approximately 3 min when the bulk water temperature was 30 °C. Measurements for the saturated cases were started 5 min after reaching the saturation state. The bulk water temperature was dropped by 0.3 and 0.2 °C between successive measurements for unsaturated and saturated cases, for the initial bulk water temperature of 36 and 30 °C, respectively. The bulk water temperatures for all cases are presented in Table 1. As the decrease in the bulk water temperature was small, the bulk water temperatures correspond to the unsaturated cases (i.e. 30 °C and 36 °C) are used as the reference for both saturated and unsaturated cases in the subsequent sections. Relative humidity in the tank was also measured at two different heights from the water surface using the humidity probes (HX92AV-D, Omega Engineering, Inc.) with an accuracy of ±2.5%. For both unsaturated cases, the relative humidity was varied from approximately 50% to 33% from a height of 4 cm to 15 cm above the water surface. The relative humidity of the room air was 30%.

The waterside two-dimensional velocity fields were measured using digital particle image velocimetry (DPIV). The measurements were made in a plane perpendicular to the water surface at the mid-tank location along the longer tank dimension (i.e. 30 cm from the end) as shown in Fig. 1. A Continuum Minilite 25 mJ Nd:YAG laser was used as a light source for the DPIV measurements. A CCD camera (JAI CV-M2) with the resolution of 1600 × 1200 pixels was used to image the flow. The camera was mounted in the vertical position to allow measurements to a greater depth. That is, the images were acquired with the dimensions of 1200 pixels in horizontal and 1600 pixels in vertical, with respect to the flow field. The field of view of the camera was set equal to 6.2 cm horizontal and 8.3 cm vertical. The vertical position of the camera was set in a way that the upper edge of the image coincides with the water surface. The camera was connected to a PC equipped with a frame grabber (DVR Express, IO Industries, London, ON, Canada) that acquired 8-bit images at a rate of 30 Hz. The water was seeded with silver-coated glass spheres, with the mean diameter of 15 μm (Potter Industries, Paoli, PA). These glass spheres were used as tracer particles for DPIV measurements. A four-channel digital delay generator (555-4C, Berkeley Nucleonics Corporation, San Rafael CA) was used to control the timing of the laser light pulses. For each experimental run, the data was acquired for 5 min.

Total heat loss per unit area (q''_{total}) from the tank was computed for both saturated and unsaturated cases in a separate set of experiments. For unsaturated case, heat loss was measured by measuring the rate of decrease of the bulk water temperature that is, $\frac{dT_b}{dt}$ in the mid plane depth for

Table 1
T_b, bulk water temperature; q''_{total}, total heat flux; q''_s, heat flux through the water surface; q''_{sensible}, sensible flux through the water surface; q''_{wall}, wall heat flux; w^*, velocity scale; Ra, flux-based Rayleigh number

Case	Unsaturated conditions		Saturated conditions	
T_b (°C)	36	30	35.7	29.8
q''_{total} (W/m^2)	678	367	420	211
q''_s (W/m^2)	591	309	333	153
q''_{sensible} (W/m^2)	49	26	26.4	16
q''_{wall} (W/m^2)	87	58	87	58
w^*(mm/s)	5.1	4.0	4.2	3.1
Ra	1.17×10^{12}	5.16×10^{11}	7.14×10^{11}	3.05×10^{11}

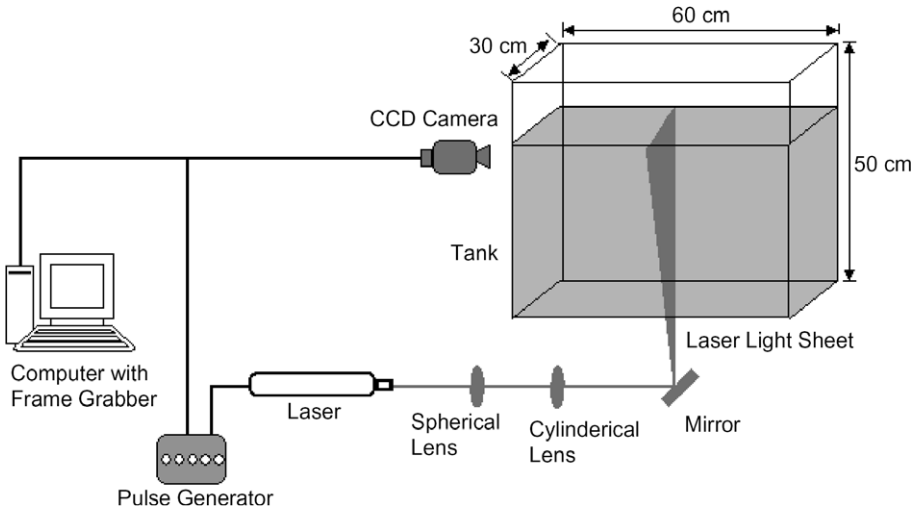

Fig. 1. Schematic of the experimental setup.

same bulk water temperatures [1]. For saturated conditions, same procedure was adopted except that the tank top was covered with a lid and the rate of decrease of the bulk water temperature was measured once 100% humidity level was reached inside the tank. The data were acquired for 15 min for each case. The q''_{total} was computed using the relation:

$$q''_{\text{total}} = \rho \times c_p \times d \times \left(\frac{\mathrm{d}T_{\text{b}}}{\mathrm{d}t}\right) \tag{1}$$

where d is the depth of water in the tank and ρ is the density of water. During these experiments, the air temperature was also measured at five different heights that varied from 4 mm to 18 cm above the water surface. The heat loss by conduction through the sidewalls and bottom was determined in another set of experiments under the identical conditions using the approach described in Katsaros et al. [3]. For these experiments, the tank was filled with water up to the rim and the top was covered with the lid of the same thickness of the glass as used on the sidewalls and bottom. The rate of decrease of the bulk water temperature was recorded and the heat loss per unit area through the sidewalls, lid and bottom of the tank was computed using the following relation:

$$q''_{\text{w}} = \rho \times c_p \left[\frac{lbd}{2(lb + bd + ld)}\right] \frac{\mathrm{d}T_{\text{b}}}{\mathrm{d}t} \tag{2}$$

where l, b, and d are the length, breadth and depth of the tank [3]. The difference between the total heat loss and the heat loss through the walls was equal to the heat flux from the free surface (q''_{s}). The values of the total and surface heat fluxes for both experimental conditions are given in Table 1. The flux based Rayleigh number was computed using the surface heat flux estimates. The values of Rayleigh number for all cases are also given in Table 1.

The temperature during experiments was measured with the thermistors (TJ 72-44033, Omega Engineering, Inc.) with an accuracy of 0.1 °C. The thermistors were calibrated using Traceable Digital Thermometer (Control Company USA) which has resolution of 0.001 °C with ±0.05 °C accuracy. The temperature data was acquired via a 16-channel data acquisition card (PCI-6036E, National Instruments) using the LabView data acquisition software.

The DPIV technique computes the velocity vectors by cross-correlating the interrogation region in the first image with the corresponding search region in the second image of an image pair. In the present study, the size of the interrogation region was set equal to 32 × 32 pixels and the size of the search region was set equal to 64 × 64 pixels. A 50% window overlap was used in order to increase the nominal resolution of the velocity field to 16 × 16 pixels. This resulted in the spatial resolution of 0.83 × 0.83 mm of the velocity field. For all cases, the velocity vectors nearest to the surface were located 1.65 mm below the air–water interface. A scheme was used to identify the spurious velocity vectors and then correct them using a local median test [6]. Typically, 1% of the velocity vectors were spurious. The uncertainty in the velocity measurements was estimated to be less than 6% for the unsaturated case [1] and less than 9% for the saturated case. For each unsaturated case, 2250 velocity fields were obtained at 7.5 Hz [1] and for each saturated case, 1125 velocity fields were obtained at 3.75 Hz (i.e. the total sampling time of each case was 5 min).

3. Results and discussion

The values of surface heat flux for saturated and unsaturated cases are tabulated in Table 1 for both bulk water temperatures. The results show that for the given bulk water temperature, the surface heat flux for the unsaturated case was larger than the saturated one. When the air became saturated, the surface heat flux was decreased by 43% and 50% for the bulk water temperatures of 36 °C and 30 °C, respectively. The surface heat flux constitutes both the sensible and latent fluxes. The surface sensible heat flux depends on the airside heat transfer coefficient and the surface to bulk air temperature difference. The heat transfer coefficient for air during natural convection was computed using standard correlation for the free convection from the horizontal surface [7]. The air temperatures at 4 mm and 18 cm heights from the water surface were used as the reference temperatures with the assumption that the air temperature at 4 mm is approximately the same as the surface temperature. The values of the surface sensible heat flux for all cases are presented in Table 1. The sensible heat fluxes found to be approximately 8–10% of the total surface heat flux, which is in the same range as in the previous studies [2,3]. The estimate of the latent heat flux was obtained by subtracting the surface sensible heat flux from the total surface heat flux.

Comparison of the estimated latent heat flux for saturated and unsaturated cases shows that the latent heat flux for the saturated case is approximately 40% and 50% lower than that for the unsaturated case at the bulk water temperatures of 36 °C and 30 °C, respectively. It is typically assumed that the latent heat flux is very small or negligible when the air is saturated. The above results show that in the present study, the latent heat flux is quite significant at the saturation state. We searched through the literature but could not find any study that actually estimated the surface heat flux at the saturation condition, for comparison. The results in Table 1 provide the first estimation of the surface heat flux at saturation state and showed that for the present setup, it is significant. The physical explanation of the observed latent heat flux at saturation state is provided below.

For unstably stratified conditions, when the bulk water is warmer than air, there is a sensible heat transfer from water to air, in addition to the latent heat flux. For these thermally unstable conditions, when the tank top was open, due to the exchange of air masses between the tank and the surroundings by convective motion, the bulk air temperature inside the tank remained same as the room

air temperature. However, for the saturated case when the lid was closed, the warmer air above the water surface was not replaced by the cool air from outside, which resulted in an increase in the air temperature inside the tank. The temperature measurements on the airside have shown that at a height of 18 cm from the water surface for saturated air conditions, the air temperature was increased by 4 °C and 2 °C compared to the room air temperature, for 36 °C and 30 °C cases, respectively. In this situation, the top lid and the side walls that bound the air acted as cold surface. The water vapors in air when came in contact with this surface, released the heat of condensation and deposited on the surface in the form of condensate film [8]. As the vapor condensed on the top lid and side walls, the same amount of water vapor was taken up by the air from water to maintain the saturation state. This process occurred in the quasi-steady form that is, a continuous film condensation resulted in a continuous mass transfer from water to air to replenish the vapor loss from air. Thus, a net latent heat transfer occurred from water to air, as observed in the present study. Thus, it can be concluded that the air saturation during unstably stratified conditions, resulted in a net latent heat flux transfer from water to air due to the vapor condensation at the tank boundaries.

Another factor that contributes to the latent heat transfer during saturation state is the bulk air–water temperature difference. As mentioned earlier, during unstable stratification when the water is warmer than air, there is a sensible heat transfer from water to air which resulted in an increase in the air temperature. An increase in the air temperature increases the saturation pressure of vapor in air. This allows more moisture to be added to air resulting in the latent heat transfer. The present study provided the evidence of the latent heat transfer at the saturation state. However, detailed velocity and temperature measurements on the airside during saturation state are necessary in order to improve our understanding about the heat transfer process across the air–water interface at this state.

As mentioned above, at the saturation state the temperature of air was increased by 4 °C and 2 °C for 36 °C and 30 °C cases, respectively. This resulted in a reduction in the sensible heat flux through the surface. This is evident in the surface sensible heat flux values in Table 1, which shows that as the air became saturated, the surface sensible heat flux was reduced by 40–45%.

The horizontal and vertical root-mean-square (RMS) turbulent velocities are plotted in Fig. 2a and b, respectively, as a function of depth for saturated and unsaturated cases. Fig. 2a shows that for both saturated and unsaturated cases, the variation in the horizontal velocity with depth is relatively small. For unsaturated cases, the profiles show that the horizontal turbulent velocities increased within a depth of approximately 5 mm and then started decreasing to a certain depth after that became almost constant. The profiles for the saturated case also show a similar trend in the near-surface region. However, the increment in the horizontal velocity within 5 mm for the saturated case is relatively very small compared to the unsaturated case. Comparison of the depth-averaged velocity magnitude between the saturated and unsaturated cases shows that the horizontal turbulent velocity for unsaturated case is a factor of 5.8 and 4.6 higher than that for the saturated case at the bulk water temperatures of 30 °C and 36 °C, respectively.

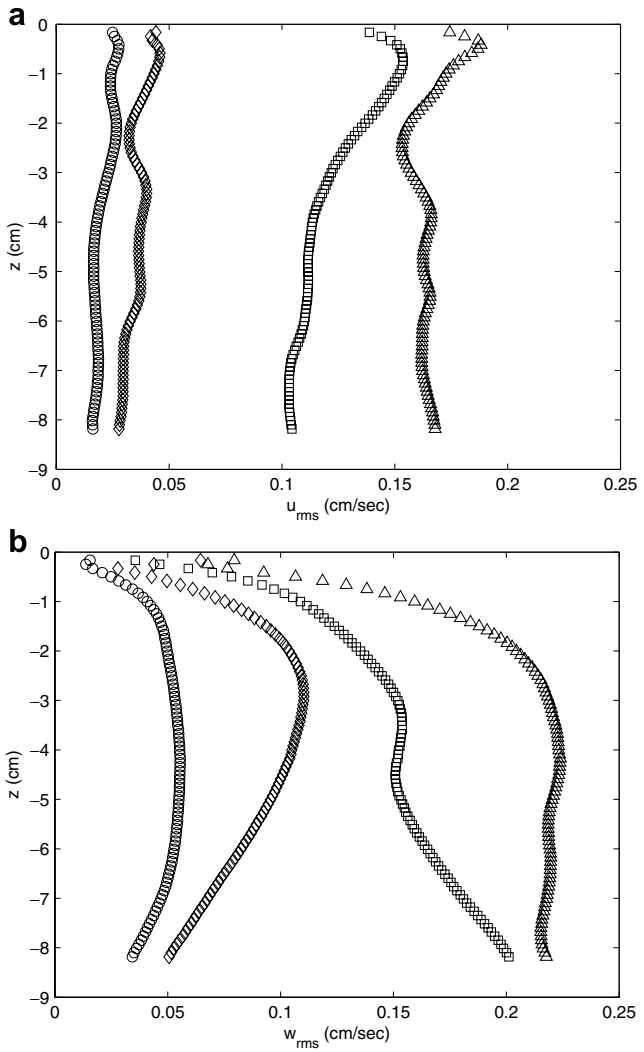

Fig. 2. Vertical profiles of the RMS turbulent velocities: (a) horizontal, (b) vertical. (○) 30 °C (saturated); (□) 30 °C (unsaturated) [1]; (◇) 36 °C (saturated); (△) 36 °C (unsaturated) [1].

The air–water interface is a shear-free boundary with the slip boundary condition for the horizontal velocity. That is, the horizontal motions exist at the water surface. The plot in Fig. 2a shows that for the saturation case the horizontal motions immediately below the water surface are a factor of 5 and 4 smaller than that for the unsaturated case for the bulk water temperature of 30 °C and 36 °C, respectively. Bukhari and Siddiqui [4] simulated the air and water velocity fields during natural convection. They have shown that for the bulk water temperatures of 37 °C and 32 °C, and the bulk air temperature of 22 °C, the RMS airside velocity was more than an order of magnitude larger than

the waterside RMS velocity. The strong motion on the airside influences the waterside velocity field via the common boundary (i.e. the air–water interface). The strong motions on the airside increase the horizontal velocity at the common boundary. This velocity at the boundary influences the velocity field on the waterside.

On the airside, the temperature and vapor concentration differences between the surface and bulk influence the velocity field [9]. For the unsaturated case, as the water evaporates it diffuses upward through the air and at steady state this upward movement must be balanced by a downward diffusion of dry air so that the concentration at any height remains constant. If the air column above the water surface is wide enough, the humid air rises by natural convection through the center of the column and the dry air descends along the walls [10]. Bukhari and Siddiqui [4] also observed similar bulk airflow pattern from simulations. For the saturated case, the mass transfer is controlled by the film condensation simultaneously occurring at the side walls and the top lid. The airflow pattern for this case is not known, however, it is expected to be different from that for the unsaturated case and would be much more complicated. Thus, the pattern of mass diffusion on the airside in both cases would be different. The concentration gradient and surface to bulk temperature difference on the airside for the saturated case would be much lower than that for the unsaturated case. Thus, a significant reduction in the air velocity magnitude is expected at the saturation state, which causes a substantial reduction in the horizontal velocity magnitude at and beneath the water surface as observed in Fig. 2a. Thus, it can be concluded that during natural convection in a coupled air–water system, the waterside velocity field is also influenced by the airside velocity field in addition to the waterside bulk-to-surface temperature difference.

Fig. 2a shows that for almost all cases, the shape of the profiles changes at depths less than 3 cm. That is, the velocity magnitude decreases up to a depth of approximately 3 cm and then it remains almost constant at greater depths. As discussed earlier, the strong airside velocity field influences the waterside velocity field by inducing horizontal velocity at the boundary. For the unsaturated case, the airside horizontal velocity is more than an order of magnitude larger than the waterside horizontal velocity [4]. Thus, for waterside, the horizontal velocity at the interface is expected to be large. Beneath the air–water interface, the horizontal velocity field is the superposition of the horizontal velocity field due to the interface velocity and the horizontal velocity field due to the convective motion induced by the waterside bulk to surface temperature difference. As the depth increases, the horizontal velocity induced by the interface decreases. For unsaturated cases, since the magnitude of the interface induced horizontal velocity is expected to be large in the near-surface region, the overall effect is a decrease in the horizontal velocity with depth in the near-surface region. As greater depths, the horizontal velocity field due to the convective motion would be more dominant and the variation in the horizontal velocity magnitude is minimal within the given depth. For the saturated cases as discussed earlier, the air velocity magnitude would be significantly smaller and thus, the magnitude of the horizontal velocity field induced by the interface velocity would also be small and thus, the decrease in horizontal velocity within in the near-surface region is relatively small.

Fig. 2b shows a sharp increase in the vertical component of the turbulent velocity with depth for all cases. For unsaturated cases, the plot shows that the vertical turbulent velocity increased rapidly up to a depth of approximately 3 cm and then it remains almost constant to a certain depth. For the bulk water temperature of 30 °C, the plot shows that the vertical turbulent velocity increased at greater depths. However, for the higher bulk water temperature (36 °C), it remained almost constant within the measurement depth. For the saturated cases, the plot shows that the vertical turbulent velocity increased with depth similar to the unsaturated cases, but as the depth further increased, the magnitude of the vertical velocity tends to decrease. Comparison between saturated and unsaturated cases show that similar to the horizontal turbulent velocity, the vertical turbulent velocities are larger in magnitude for unsaturated cases for the same bulk water temperatures. In the depth range 3–4 cm from the water surface where the largest increase in the vertical turbulent velocity was observed, the magnitude of the vertical turbulent velocity for the unsaturated case was a factor of 2 and 2.8 higher than that for the saturated case at the bulk water temperatures of 36 °C and 30 °C, respectively. For both 36 °C and 30 °C cases, the surface heat flux was a factor of 1.9 and 2.2 higher when the air was unsaturated. High heat transfer through the surface makes the water surface layer cooler and denser which starts falling deep into the water more vigorously than that for the saturated conditions for the same bulk water temperatures. In other words, the surface to bulk temperature gradients would be larger and could exist up to greater depths. For the saturated cases, the velocity increased sharply in the near-surface region and then after a short distance it started to decrease. This change in the shape of the profiles indicates that the temperature gradient exists over relatively shorter depth. Thus, the flow accelerates over a shorter distance from the interface and then started to decelerate and the vertical convective motions become very weak. Furthermore, the horizontal velocity magnitude at the interface is also significantly different for saturated and unsaturated cases, which would also influence the vertical velocity field.

Table 1 shows that the surface heat flux for the saturated case at 36 °C is slightly larger than that for the unsaturated case at 30 °C. However, the magnitude of the horizontal turbulent velocity is significantly lower for the former and the vertical turbulent velocity of the former is about 30% less than the latter in 3–4 cm depth range. The significant difference in the horizontal turbulent velocity magnitude is likely due to the significant reduction in the air velocity during the saturation case. The comparable magni-

tudes of the vertical velocity within 5 mm from the surface and the surface heat fluxes for both cases indicate that the vertical density gradients in the near-surface region could also be comparable for both cases. The decrease in the vertical velocity magnitude at greater depths for the 36 °C saturation case could be due to the reason that at greater depth the magnitude of the vertical density gradients is lower than that for the 30 °C unsaturated case. Detailed waterside temperature measurements in the vertical plane would provide better explanation for this behavior.

The comparison of plots in Fig. 2a and b shows that for all cases, in the near-surface region, the magnitude of the horizontal velocity is significantly large compared to the vertical turbulent velocity. However, away from the surface, the magnitude of the vertical turbulent velocity is larger than the horizontal turbulent velocity. This is due to the reason that in the near-surface region, the horizontal velocity is influenced by the velocity at the interface which is controlled by the airside motion and the vertical velocity approaches zero at the interface. At greater depths, the vertical turbulent velocity increases due to the strong vertical convective motion in the form of rising plumes and falling sheets [1,2].

Adrian et al. [11] proposed scaling parameters for the fluid bounded by the solid walls undergoing thermal convection when heated from below. They defined the length scale as water depth denoted by z^*, and the velocity scale is defined as

$$w_* = (\beta g Q_0 z_*)^{1/3} \tag{3}$$

where β is the thermal coefficient of expansion, g is the acceleration due to gravity and Q_0 is the kinematic heat flux defined as

$$Q_0 = \frac{q_s''}{\rho c_p} \tag{4}$$

where q_s'' is the surface heat flux, ρ is the density and c_p is the specific heat. They argued that this scaling is applicable in the regions where the flow is dominated by convection, which covers almost the entire fluid domain except a very thin layer adjacent to the solid wall where conduction is the primary mode of heat transfer. Bukhari and Siddiqui [1] showed that this scaling is also applicable to the flow beneath air–water interface undergoing evaporation when the air is unsaturated. The values of w^* for all cases are presented in Table 1. The RMS horizontal and vertical turbulent velocities normalized by w^* are plotted in Fig. 3a and b, respectively, versus the normalized depth. For both unsaturated cases, the data collapsed into a relatively narrow band [1], however, for the saturated cases, the data collapsed well only in certain range. The plots show the horizontal turbulent velocity for the saturated cases collapsed reasonably well for $z/z^* < 0.1$, whereas, the vertical velocity collapsed well for $z/z^* < 0.03$ and $z/z^* > 0.2$.

The profiles in Figs. 2b and 3b also show that there is an increase in the vertical velocity very close to the interface (i.e.

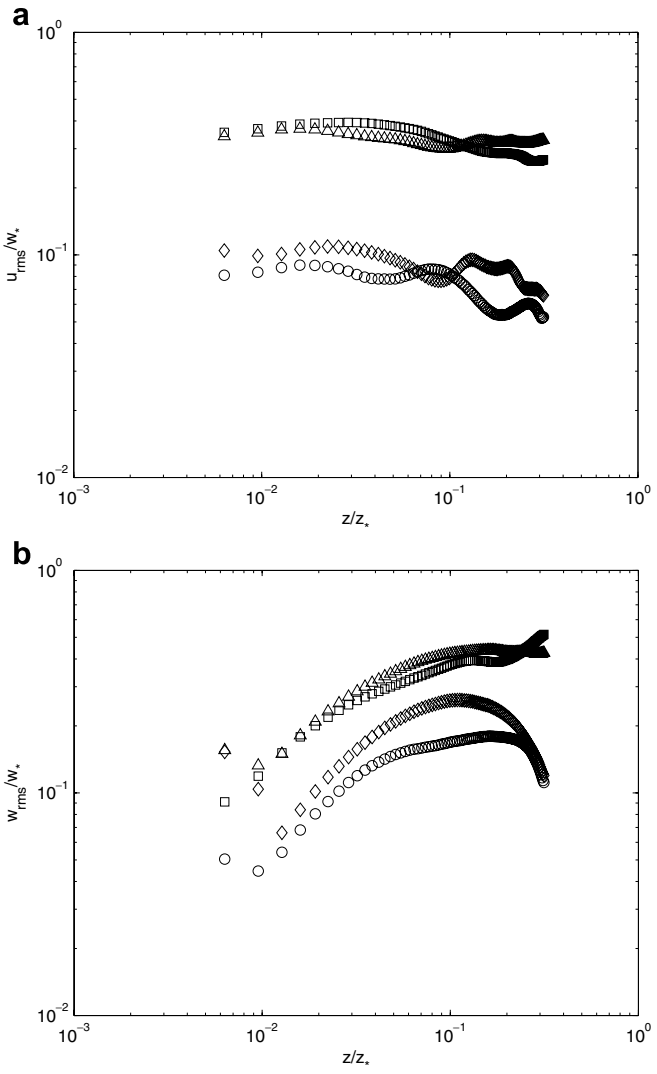

Fig. 3. Vertical profiles of the RMS turbulent velocities normalized by w^*: (a) horizontal, (b) vertical. (○) 30 °C (saturated); (□) 30 °C (unsaturated) [1]; (◇) 36 °C (saturated); (△) 36 °C (unsaturated) [1].

within the range $z < 5$ mm or $z/z^* < 0.02$) for all cases except the unsaturated case at 30 °C. The vertical velocity is expected to decrease as it approaches the interface due to the no-penetration boundary condition. Katsaros et al. [3] proposed a model for the thermal boundary layer beneath the air–water interface during natural convection. According to this model, there is a thin layer at the water surface where the heat is transferred due to molecular diffusion. Beneath this layer, there is another layer which they termed "Thermal source layer" that acts as a source for the cold water to produce falling sheets. They argued that within this layer the cold water is replaced by the rising warm water that results in a net upward warm advection into this region. Thus, the vertical velocity component due to the vertical advection could be relatively large in this layer. They predicted the depth of the thermal source layer to be about 1.25 mm, for surface heat flux of 210 W/m^2. Thus, an increase in the vertical velocity near the interface in the present study indicates the existence of the thermal source layer.

The profiles in Figs. 2b and 3b show that for the case of 36 °C, the thickness of the thermal source layer for the unsaturated case is 2.5 mm and for the saturated case is 3.3 mm. Similarly, for the bulk water temperature of 30 °C, the thermal source layer was not observed for the unsaturated case which could be due to reason that the thickness of this layer is smaller than the velocity resolution. For the saturated case, the thickness of the layer is 2.5 mm. The trends at both 30 °C and 36 °C indicate that for the given bulk water temperature, the thickness of the thermal source layer is increased for the saturated case. However, this behavior is not consistent with the trend for a given saturated or unsaturated case, as the heat flux decreased (i.e. the bulk temperature changed from 36 °C to 30 °C), the thickness of the thermal source layer also decreased. This discrepancy could be due to the reason that some other parameter(s) which is influenced by the saturation would play an important role in controlling the thickness of the thermal source layer. For example, for a given bulk water temperature, the surface temperature and the bulk-to-surface temperature difference would change when the air become saturated. This would change the temperature difference across the conduction layer which would influence the thermal source layer. The detailed dynamics within the thermal source layer are not well understood. Katsaros et al. [3] presented a conceptual model of this region based on the comparison of their temperature profiles with the theoretical conduction profiles. Detailed and high-resolution velocity and temperature measurements in this region are necessary to understand flow dynamics in this layer.

The turbulent kinetic energy (TKE) is plotted in Fig. 4 as a function of depth for saturated and unsaturated cases. As seen in Fig. 2, except in the region adjacent to the interface, the magnitude of the horizontal turbulent velocity is smaller than the vertical turbulent velocity and also the variation in the horizontal velocity with depth is relatively small. Therefore, the shape and magnitude of the TKE profiles is dominated by the behavior of the vertical turbulent velocity. In the depth range 3–4 cm, the magnitude of TKE for the unsaturated case is a factor of 17 and 9 larger than that for the saturation case for the bulk water temperatures of 30 °C and 36 °C, respectively. Similar to the vertical turbulent velocity, the TKE for the saturation case starts decreasing with depth within a short distance from the interface. This indicates that for the saturation case, the flow accelerates to a shorter distance from the interface and then starts decelerating. That is, the falling sheets accelerate as they plunge into the deeper layer but within a short distance they become weak. However, for the unsaturated case, the falling sheets accelerate as they plunge into the deeper water to much greater depths. This indicates that the flow mixing for the saturated cases is restricted to a relatively small region near the interface. As discussed earlier, small density gradients for the saturated cases could be responsible for this behavior.

Bukhari and Siddiqui [1] conducted a detailed spectral analysis of the length and time scales of the turbulent

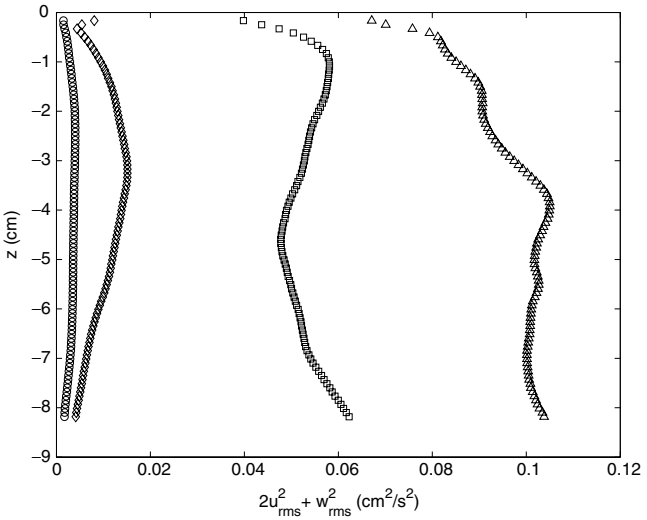

Fig. 4. Vertical profiles of the mean turbulent kinetic energy. (○) 30 °C saturated; (□) 30 °C (unsaturated) [1]; (◇) 36 °C (saturated); (△) 36 °C (unsaturated) [1].

motions for the unsaturated case. They observed the existence of the buoyancy subrange within the inertial subrange where the turbulent kinetic energy is removed by working against the buoyancy forces [12]. This was the first evidence of the existence of the buoyancy subrange beneath air–water interface during natural convection. They observed buoyancy subrange in the spectra of the horizontal velocity at all depths. However, for the vertical velocity, no buoyancy subrange was observed in the near-surface region for the higher heat flux. They argued that the buoyancy subrange exits only when the turbulence is strong enough to work against the buoyancy forces. They also found that the range of the length scales of the turbulent motions involved in the interactions with the buoyancy forces does not vary with the heat flux. However, the range of timescales of the turbulent motion reduces with a decrease in the heat flux.

The wavenumber spectra of the horizontal and vertical turbulent velocities were computed for all cases. The one-dimensional wavenumber spectrum was computed in the horizontal direction at all depths in each velocity field and then averaged at each depth. The wavenumber spectra of the horizontal velocity for the saturated and unsaturated cases are shown in Figs. 5a, 6a and 7a at depths of 0.33, 2.9 and 8.0 cm, respectively. The spectra are normalized by w^* and z^*. The results in Figs. 5a, 6a and 7a show that for the saturated case the buoyancy subrange was observed at all depths. However, the range of wavenumbers over which the buoyancy subrange was observed was smaller than that for the corresponding unsaturated cases. The plots also show that for the saturated case, the range of wavenumbers over which the buoyancy subrange was observed decreased with a decrease in the bulk water temperature. The plots also indicate that with an increase in depth, the buoyancy subrange became shorter and shifted towards the low wavenumbers. That is, as the overall horizontal turbulent

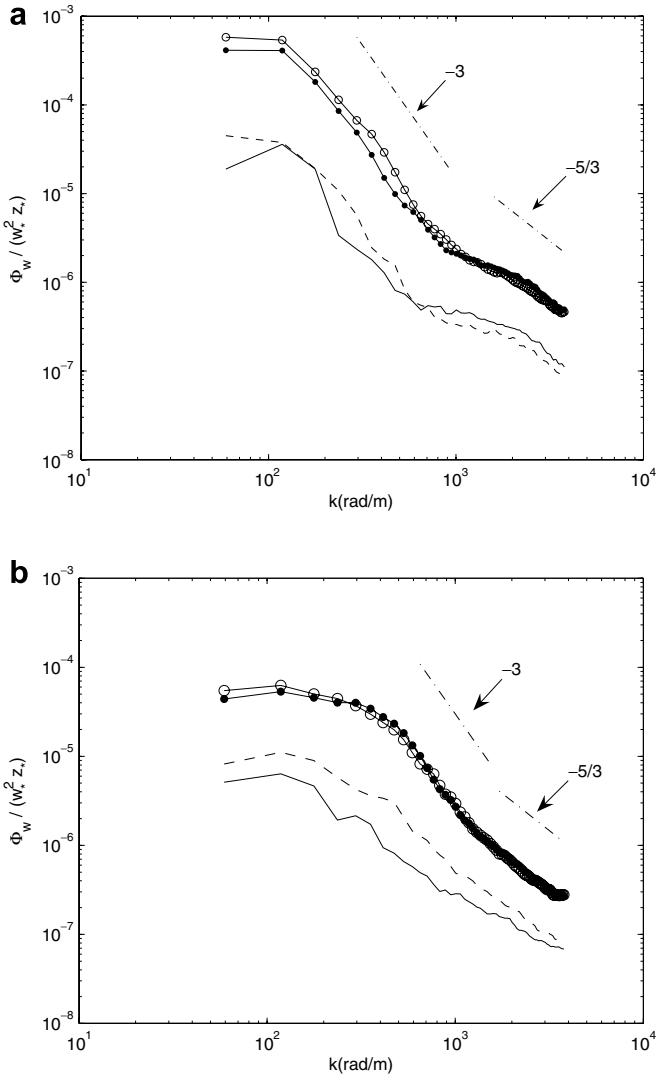

Fig. 5. Normalized wavenumber spectra of the turbulent velocities: (a) horizontal, (b) vertical, at depth $z = 0.33$ cm. (○) 36 °C (unsaturated); (●) 30 °C (unsaturated); (dashed line) 36 °C (saturated); (solid line) 30 °C (saturated). Dashed-dotted lines represent slopes.

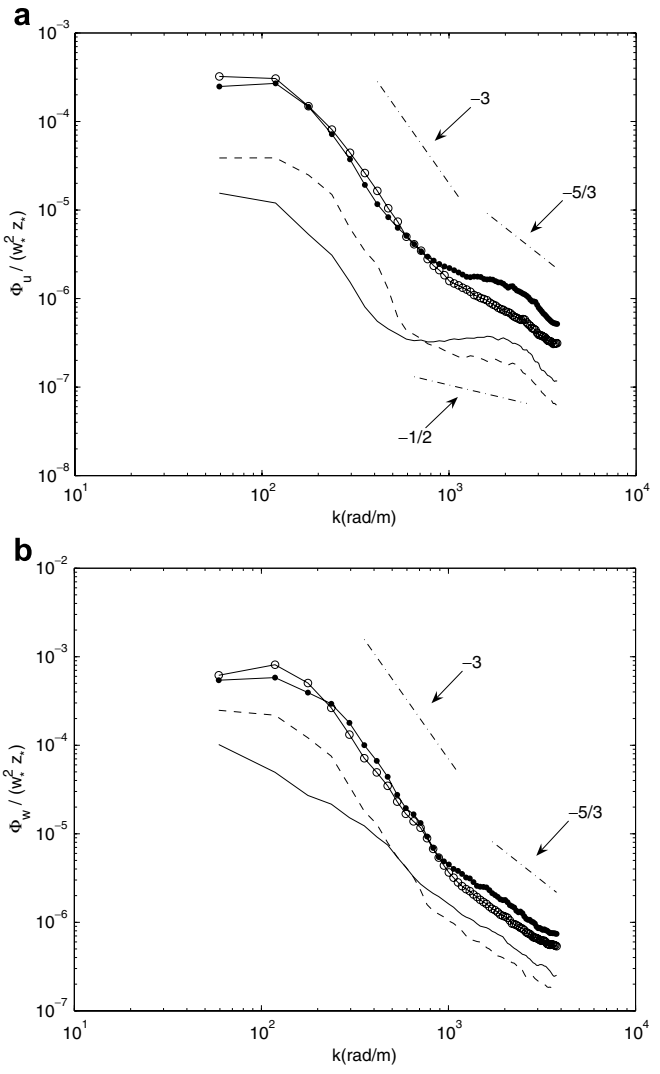

Fig. 6. Normalized wavenumber spectra of the turbulent velocities: (a) horizontal, (b) vertical, at depth $z = 2.9$ cm. (○) 36 °C (unsaturated); (●) 30 °C (unsaturated); (dashed line) 36 °C (saturated); (solid line) 30 °C (saturated). Dashed-dotted lines represent slopes.

motions became weaker with depth, only a small range of relatively larger and energetic turbulent motions were able to work against buoyancy.

The wavenumber spectra of the vertical velocity for the saturated and unsaturated cases are shown in Figs. 5b, 6b and 7b at depths of 0.33, 2.9 and 8.0 cm, respectively. For the saturated cases, no buoyancy subrange was observed at the depth of 0.33 cm. This is due to the reason that the turbulence is not strong enough to work against the buoyancy forces [1]. At a depth of 2.9 cm where the vertical velocity magnitude is largest for the saturation cases, the buoyancy subrange was observed for 36 °C case but not for the 30 °C. However, at a depth of 8.0 cm where the vertical turbulent velocity magnitude is very small, the buoyancy subrange is manifested at both bulk water temperatures. The presence of the buoyancy subrange at this depth indicates that the buoyancy forces are very weak at this depth and the turbulent intensity (which is relatively weak itself) is strong enough to work against the buoyancy forces. Similar to the horizontal velocity spectra, the wavenumber range for the buoyancy subrange is shorter for the saturated case compared to the unsaturated case.

In Figs. 5a, 6a and 7a, the inertial subrange was observed at wavenumbers greater than 1500 rad/m. The plots show that the wavenumber range for the inertial subrange is almost the same for both saturated and unsaturated cases and at both bulk water temperatures. This indicates that scales of the horizontal turbulent motions at which the conventional energy transfer takes place is not influenced by the airside relative humidity or the bulk water temperature. An interesting feature that was observed in the horizontal velocity spectra is that the buoyancy subrange is separated from the inertial subrange. For the unsaturated cases, there is some indication of this separation for the 30 °C case. However, for the saturated cases, this trend is more obvious at both bulk water

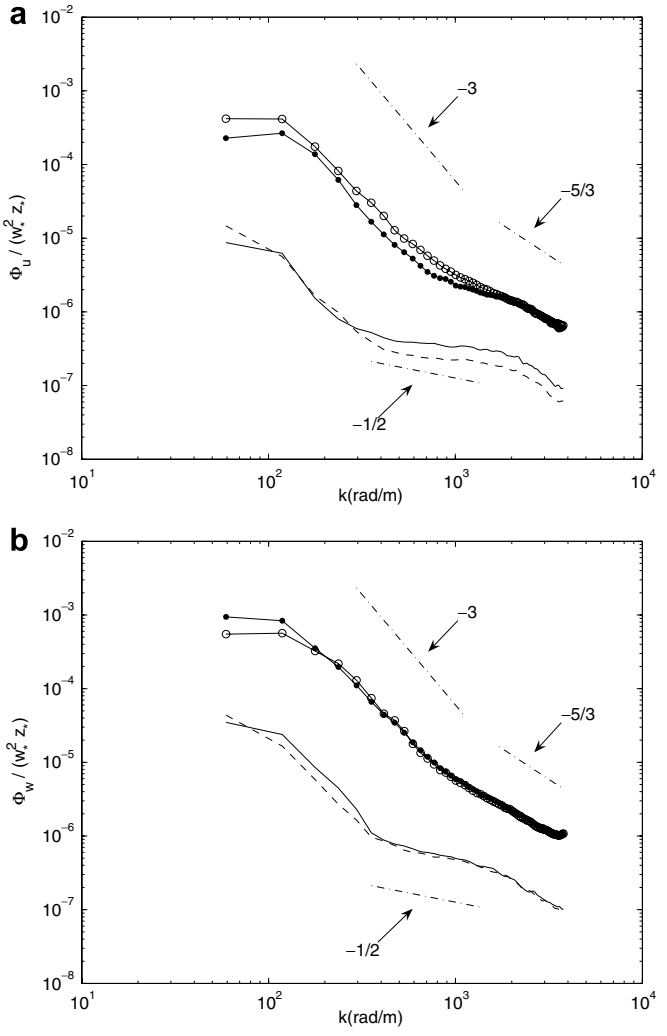

Fig. 7. Normalized wavenumber spectra of the turbulent velocities: (a) horizontal, (b) vertical, at depth $z = 8.0$ cm. (○) 36 °C (unsaturated); (●) 30 °C (unsaturated); (dashed line) 36 °C (saturated); (solid line) 30 °C (saturated). Dashed-dotted lines represent slopes.

temperatures. As discussed earlier, for the saturated case, the wavenumber range over which the buoyancy subrange exists decreased towards the low wavenumbers. Since the wavenumber range of the inertial subrange remains unchanged, the buoyancy subrange is separated from the inertial subrange as it is shifted towards the low wavenumbers. In the spectra of the vertical velocity, this separation was not observed for the unsaturated case. For the saturated case, it was observed only at a depth of 8 cm (see Fig. 7b). In the wavenumber range that separates the two subranges, the spectra exhibits a slope of $-1/2$. Turner [12] argued that the buoyancy subrange exists within the inertial subrange. This implies that the slopes of both subranges should merge within a small range of wavenumbers as evident in the vertical velocity spectra and also in the horizontal velocity spectra for unsaturated case at 36 °C. The existence of the third subrange where the spectra exhibits $-1/2$ slopes implies that the energy transfer mechanism in this range is different from the other two ranges. The small slope in this range indicates that the energy transfer at these scales is significantly slower than that in the buoyancy and inertial subranges. In this range, the turbulence is too weak to work against the buoyancy forces and, the dissipation rate is not the controlling parameter for the energy transfer. Thus, it can be argued that in buoyancy-driven flows, when the turbulence is relatively weak, in addition to the buoyancy subrange, another subrange exists within the inertial subrange, where the turbulent motions are simply convected by the buoyancy forces. Detailed information about the density gradients and buoyancy forces is necessary in order to provide the physical explanation for the manifestation of this subrange, which is beyond the scope of the present work.

The physical mechanism of the energy interaction beneath air–water interface when the air is saturated can be described as follows. Both the horizontal and vertical turbulent motions are much weaker than that for the unsaturated case. Therefore, the buoyancy subrange was not observed for all cases. For the cases where the buoyancy subrange was observed, it was found that the wavenumber range of buoyancy subrange decreased with depth. That is, as the depth increased, only larger turbulent motions were able to work against the buoyancy. In other words, at smaller depths (i.e. near the surface), there is a range of turbulent motions at relatively higher wavenumbers that were strong enough to work against buoyancy but at greater depths, these turbulent motions became so weak that they were not able to work against buoyancy and simply advected by the buoyancy forces. Thus, it can be concluded that the energy interaction is highly dependent on the energy of the turbulent motions and the magnitude of the buoyancy forces.

4. Conclusions

The impact of the air saturation on the turbulent structure beneath the air–water interface has been investigated. The results show that air saturation has a significant impact on the waterside turbulent structure. As the air becomes saturated, the magnitudes of the horizontal and vertical turbulent velocities are decreased on average, by factors of 5 and 2.5, respectively; and the horizontal motions at the water surface are reduced by a factor of 4 to 5. The significant reduction in the waterside velocities is attributed to the reduction in the surface heat flux, airside velocities and the waterside vertical density gradients during the saturation state. It is observed that the latent heat flux at the saturation state is not equal to zero. The film condensation on the tank walls at the saturation state is found to be responsible for the latent heat flux. The spectral analysis shows that both the horizontal and vertical turbulent motions are much weaker than that for the unsaturated case. For the saturated cases, the range of the turbulent motions responsible for working against buoyancy forces is smaller than that for the unsaturated cases. Furthermore, with an increase in depth, only larger

turbulent motions within this range work against the buoyancy and the remaining smaller turbulent motions in the range are advected by the buoyancy forces. It was concluded that during natural convection, when the turbulence is relatively weak, in addition to the buoyancy subrange, another subrange exists within the inertial subrange, where the turbulent motions are simply convected by the buoyancy forces and that the energy interaction is highly dependent on the energy of the turbulent motions and the magnitude of the buoyancy forces.

Acknowledgements

This research was funded by a grant from the Natural Sciences and Engineering Research Council of Canada (RGPIN 261422-03) to M.H. Kamran Siddiqui.

References

[1] S.J.K. Bukhari, M.H.K. Siddiqui, Turbulent structure beneath air–water interface during natural convection, Phys. Fluids 18 (2006) 035106.
[2] R.J. Volino, G.B. Smith, Use of simultaneous IR temperature measurements and DPIV to investigate thermal plumes in a thick layer cooled from above, Exp. Fluids 27 (1999) 70–78.
[3] K.B. Katsaros, W.T. Liu, J.A. Businger, J.E. Tillman, Heat transport and thermal structure in the interfacial boundary layer measured in an open tank of water in turbulent free convection, J. Fluid Mech. 83 (1977) 311–335.
[4] S.J.K. Bukhari, M.H.K. Siddiqui, Characteristics of air and water velocity fields during natural convection, Heat Mass Transfer 43 (5) (2007) 415–425.
[5] K.A. Flack, J.R. Saylor, G.B. Smith, Near-surface turbulence for evaporative convection at an air/water interface, Phys. Fluids 13 (2001) 3338–3345.
[6] M.H.K. Siddiqui, M.R. Loewen, C. Richardson, W.E. Asher, A.T. Jessup, Simultaneous particle image velocimetry and infrared imagery of microscale breaking waves, Phys. Fluids 13 (2001) 1891–1903.
[7] F.P. Incropera, D.P. Dewitt, Introduction to Heat Transfer, 4th ed., John Wiley and Sons, 2001.
[8] F.P. Incropera, D.P. Dewitt, T.L. Bergman, A.S. Lavine, Fundamentals of Heat and Mass Transfer, 6th ed., John Wiley and Sons, 2006.
[9] B. Gebhart, L. Pera, The nature of vertical natural convection flows resulting from the combined buoyancy effects of thermal and mass diffusion, Int. J. Heat Mass Transfer 14 (1971) 2025–2050.
[10] A. Bejan, Heat Transfer, Wiley, New York, 1993.
[11] R.J. Adrian, R.T.D.S. Ferreira, T. Boberg, Turbulent thermal convection in wide horizontal fluid layer, Exp. Fluids 4 (1986) 121–141.
[12] J.S. Turner, Buoyancy Effects in Fluids, Cambridge University Press, 1973.